HHS Public Access

Author manuscript

Metabolism. Author manuscript; available in PMC 2022 August 01.

Published in final edited form as:

Metabolism. 2021 August ; 121: 154801. doi:10.1016/j.metabol.2021.154801.

Regulation of hepatic fibrosis by Carcinoembryonic Antigen-related Cell Adhesion Molecule 1

Raghd Abu Helal[1], **Lucia Russo**[2], **Hilda E. Ghadieh**[1], **Harrison T. Muturi**[1], **Suman Asalla**[1], **Abraham D. Lee**[3], **Cara Gatto-Weis**[1,4], **Sonia M. Najjar**[1,5,†]

[1]Department of Biomedical Sciences, Heritage College of Osteopathic Medicine, Ohio University, Athens, OH, USA

[2]Center for Diabetes and Endocrine Research (CeDER), College of Medicine and Life Sciences, University of Toledo, Toledo, OH, USA

[3]Department of Rehabilitation Sciences, College of Health Sciences, The University of Toledo, Toledo, OH, USA

[4]Department of Pathology, College of Medicine and Life Sciences, University of Toledo, Toledo, OH, USA

[5]Diabetes Institute, Heritage College of Osteopathic Medicine, Ohio University, Athens, OH, USA

Abstract

Objective: NAFLD is a complex disease marked by cellular abnormalities leading to NASH. NAFLD patients manifest low hepatic levels of CEACAM1, a promoter of insulin clearance. Consistently, *Cc1*$^{-/-}$ null mice displayed spontaneous hyperinsulinemia/insulin resistance and steatohepatitis. Liver-specific reconstitution of *Ceacam1* reversed these metabolic anomalies in 8-month-old *Cc1*$^{-/-xliver+}$ mice fed a regular chow diet. The current study examined whether it would also reverse progressive hepatic fibrosis in mice fed a high-fat (HF) diet.

Methods: 3-month-old mice were fed a high-fat diet for 3–5 months, and metabolic and histopathological analysis were conducted to evaluate their NASH phenotype.

Results: Reconstituting CEACAM1 to *Cc1*$^{-/-}$ livers curbed diet-induced liver dysfunction and NASH, including macrovesicular steatosis, lobular inflammation, apoptosis, oxidative stress, and chicken-wire bridging fibrosis. Persistence of hepatic fibrosis in HF-fed *Cc1*$^{-/-}$ treated with nicotinic acid demonstrated a limited role for lipolysis and adipokine release in hepatic fibrosis caused by *Ceacam1* deletion.

† Address correspondence to: Prof. Sonia M. Najjar, **PhD**, Department of Biomedical Sciences, Heritage College of Osteopathic Medicine, Ohio University, Athens, Ohio, 45701, Tel: (740) 593-2376, FAX: (740) 593-2778, najjar@ohio.edu.

Author contributions: L.R., H.E.G., H.T.M., K.A., S.A., A.D.L., and C.G-W. researched data; R.AH., planned and organized experiments, collected and analyzed data, and drafted the article. H.E.G., contributed to the editing of the manuscript. C.G-W. evaluated independently NAS score in mice. S.M.N. oversaw the work, including its conception and study design, analyzed data, led scientific discussions and reviewed/edited the manuscript.

Conflict of interest/Financial disclosure: None declared

Conclusions: Restored metabolic and histopathological phenotype of HF-fed *Cc1*$^{-/-\text{xliver+}}$ assigned a critical role for hepatic CEACAM1 in preventing NAFLD/NASH including progressive hepatic fibrosis.

Keywords

Hyperinsulinemia; insulin clearance; insulin resistance; nonalcoholic fatty liver disease; hepatic fibrosis

1. Introduction

Non-alcoholic fatty liver disease (NAFLD) is a complex disease encompassing a cadre of metabolic dysregulation and histological anomalies that include hepatic steatosis without or with inflammation, chicken-wire bridging fibrosis and apoptosis that advance non-alcoholic steatohepatitis (NASH) [1]. The disease is commonly associated with metabolic syndrome in light of their parallel epidemic spread worldwide [2] and of shared intertwined mechanisms underlying their pathogenesis. These include, insulin resistance, lipotoxicity, inflammation and oxidative stress [3–6].

Chronic hyperinsulinemia and insulin resistance play a critical role in the initiation and early switch from simple steatosis to NAFLD [7, 8]. This provided the impetus to use insulin sensitizers as therapeutic modalities to curb NAFLD in patients with insulin resistance in the absence of an FDA-approved drug specifically targeting fibrosis in NASH [9, 10].

Chronic hyperinsulinemia in patients with NAFLD has been attributed to impaired insulin clearance [11]. Moreover, insulin-resistant obese subjects with NAFLD manifested reduced hepatic levels of Carcinoembryonic Antigen-Related Cell Adhesion molecule 1 (CEACAM1) [12, 13], a glycoprotein that promotes receptor-mediated insulin uptake in hepatocytes followed by its degradation [14]. Consistently, mice with global [15, 16] and liver-specific [17] deletion of *Ceacam1* gene, and L-SACC1 mice with its liver-specific inactivation [18] manifested chronic hyperinsulinemia driven by impaired insulin clearance. This in turn, caused insulin resistance (due to downregulation of the insulin receptor) and hepatic steatosis (owing to increased hyperinsulinemia-driven SREBP-1c activation of lipogenic genes transcription and to the loss of insulin's repression of FASN activity mediated by CEACAM1 phosphorylation [19]). With fatty acid β-oxidation being compromised, the increase in *de novo* lipogenesis tips the balance towards fat accumulation (hepatic steatosis) and drives its redistribution to white adipose tissue (WAT) for storage (visceral obesity). In agreement with increased inflammatory response to fat accumulation, global *Cc1*$^{-/-}$ nulls developed steatohepatitis [20] in the absence of deranged cholesterol homeostasis [21]. Fed a high-fat diet, they also developed a progressive NASH-like phenotype including macrosteatosis and lipid peroxidation in addition to apoptosis and advanced fibrosis [22]. Similarly, liver-specific AlbCre+*Cc1*$^{fl/fl}$ nulls manifested NASH with advanced fibrosis when propagated on the *Ldlr*$^{-/-}$ background and fed a cholesterol-enriched diet [23].

Because CEACAM1 is expressed in all liver cells that are virtually implicated in stellate cell activation [24], and in light of the positive role of free-cholesterol lipotoxicity in

hepatocellular injury [4], the aforementioned loss-of-function models do not efficiently delineate the primary role of hyperinsulinemia caused by *Ceacam1* deletion in hepatocytes independently of altered cholesterol homeostasis. Because liver-specifc reconstitution of CEACAM1 restored insulin clearance and normal metabolism in $Cc1^{-/-}$ mice fed a regular diet [25], the current studies investigated whether it can also reverse the advanced fibrogenic NASH phenotype driven by prolonged high-fat feeding in parallel to restoring normoinsulinemia and insulin sensitivity.

2. Materials and methods

2.1. Mice maintenance

As previously described [25], mice with global *Ceacam1* deletion (C57BL/6J.$Cc1^{-/-}$ or $Cc1^{-/-}$) were bred with mice harboring liver-specific overexpression of rat *Ceacam1* transgene driven by apolipoprotein-A1 promoter (L-CC1) [26]. Genotyping was performed [25] by PCR analysis (Fig. S1) using rat and mouse specific primers (Fig. S1B). In addition to L-CC1, control littermates include $Cc1^{+/+}$ without the transgene. Only male mice were examined. All mice were kept in a 12-hour dark/light cycle and fed *ad libitum* a standard chow (RD) or a 45% high-fat (HF) diet (Research Diets, Catalog D12451, New Brunswick, NJ) for 3–5 months prior being placed in cages with Alpha-dri bedding (Shepherd Specialty Papers) and phenotyped. In some experiments, mice were injected intraperitoneally once daily with nicotinic acid (200mg/kg BW/day) (Sigma-Aldrich, St Louis, MO) for 2 days [25]. All procedures were approved by the Animal Care and Utilization Committees of participating institutions.

2.2. Insulin and glucose tolerance tests

Following a 6-hour-fast, mice were injected intraperitoneally with insulin (0.75 U/kg BW, Novo Nordisk) (for insulin tolerance) or glucose (1.5 g/kg BW of 50% dextrose solution, Dextrose Injection, USP) (for glucose tolerance). Blood was drawn from the tail vein at 0–180 min post-injection to measure glucose levels.

2.3. Whole body composition

This was assessed in live mice by nuclear magnetic resonance (Bruker Minispec, Billerica, MA, USA).

2.4. Metabolic parameters

Mice were fasted overnight and retro-orbital blood was drawn beginning at 11:00 a.m. the following morning to assess steady-state levels of plasma insulin (Mouse Ultrasensitive ELISA kit, Alpco, Salem, NH), C-peptide (ELISA, Alpco), non-esterified fatty acids (NEFA C kit, Wako Diagnostics, Richmond, VA), triacylglycerol (Pointe Scientific Triglyceride), endothelin-1 (ELISA kit, ab133030, Abcam, Cambridge, MA), TNFα (SimpleStep ELISA kit, ab208348, Abcam) and IL-6 (ELISA Kit, ab222503, Abcam). Hepatic triacylglycerol was measured as previously described [26], hepatic nitric oxide (NO) levels using Nitrate/Nitrite Fluorometric Assay (780051, Cayman Chemical, Ann Arbor, MI), and hepatic levels of reduced glutathione (GSH) were measured using the Bioxytech GSH-400 kit (OXISResearch, Portland, OR). Plasma Alanine Transaminase (ALT) (ab105134, Abcam)

and Aspartate Aminotransferase (AST) (ab105135) colorimetric assays kits were used to assess liver function.

2.5. Liver histology

Hematoxylin-eosin (H&E) was performed on formalin-fixed, paraffin-embedded liver sections. Deparaffinized and rehydrated slides were stained with 0.1% Sirius Red (Sigma, Direct Red 80) to assess fibrosis using the Brunt Criteria for scoring, as described [27].

2.6. Fatty acid synthase activity

Frozen livers were homogenized and the supernatant was added to a reaction mix containing 0.1μCi [^{14}C] malonyl-coenzyme A (Perkin-Elmer, Akron, OH) [19]. 1:1 chloroform: methanol solution was added to stop the reaction, and fatty acid synthase activity was calculated as counts/min of [^{14}C] incorporated/μg cell lysates.

2.7. Ex-vivo palmitate oxidation

Livers were homogenized before being incubated in 0.2mM of [1-^{14}C] palmitate (0.5 mCi/ml) (American Radiolabeled Chemicals, St Louis, MO), as described [25]. Perchloric acid was added to stop the reaction and recover the radioactive acid soluble metabolites. Trapped CO_2 radioactivity and partial oxidation products were measured using liquid scintillation. The oxidation rate was expressed as the sum of complete and partial fatty acid oxidation expressed in nmoles/g/min.

2.8. Western blot analysis

Livers were lysed and analyzed by SDS-PAGE followed by immunoprobing with polyclonal antibodies against phospho-Smad2 (Ser465/467), phospho-Smad3 (Ser423/425), Smad-7, α-SMA, CHOP, phospho-Stat3 (Y705), phospho-NF-κB (S536), phospho-eNOS (Ser 1177), phospho-PKCζ (phosphothreonine-Thr 410/403) (Cell Signaling, Danvers, MA, and custom-made rabbit polyclonal 3759 against mouse CEACAM1, and custom-made rat CEACAM1 (αP3[Y488]) [25]. For normalization, proteins were probed with polyclonal antibodies against Smad 2, Smad3, Stat3, NF-κB, eNOS, PKCζ and Tubulin (Cell Signaling) using parallel gels. Blots were incubated with horseradish peroxidase-conjugated donkey anti-rabbit IgG or sheep anti-mouse IgG antibody (GE Healthcare Life Sciences, Amersham, Marlborough, MA) and proteins were visualized using ECL (Amersham).

2.9. Real-time quantitative RT-PCR

Total RNA was isolated from livers with NucleoSpin RNA Kit (740955.50, Macherey-Nagel, Bethlehem, PA) and from white adipose tissue using TRIzol Reagent (15596026, Ambion, Life Technologies, CA). cDNA was synthesized by iScript cDNA Synthesis Kit (Bio-Rad Life Science, Hercules, CA), using 1μg of total RNA and oligodT primers. cDNA was evaluated with semi-quantitative RT-PCR (qRT-PCR; StepOne Plus, Applied Biosystems), and mRNA was normalized to GAPDH (for regular diet fed mice), 18S (for high-fat fed mice) or 36B4 (for white adipose tissue regardless of diet). using primers listed in Table S2.

2.10. Statistical analysis

Data were analyzed by one-way analysis of variance (ANOVA) with Tukey's for multiple comparisons using GraphPad Prism 7 software. $P<0.05$ was considered statistically significant.

3. Results

3.1. Rescuing hepatic CEACAM1 expression in Cc1$^{-/-}$ mice restored insulin clearance and sensitivity in mice fed a high-fat diet

Western blot analysis of liver lysates detected transgenic rat, but not endogenous mouse CEACAM1 in RD-fed and HF-fed *Cc1*$^{-/-\text{xliver+}}$ mice (Fig. 1A). Using rat- and mouse-specific primers (Fig. S1B; Table S2), qRT-PCR detected mRNA of transgenic rat Ceacam1 in the liver, but not in the hypothalamus, skeletal muscle or WAT of *Cc1*$^{-/-\text{xliver+}}$ mice (Table S1).

As Table 1 shows, liver-specifiic CEACAM1 reconstitution reversed total fat and plasma NEFA, and restored lean mass in 6-month-old RD-fed *Cc1*$^{-/-}$ mice (Table 1), as expected from the previously reported effect on 8-month-old mice [25]. It exerted a similar protective effect when mice were fed HF for 3 (Table 1) and 5 months (not shown). Consistent with a key role for CEACAM1 in promoting insulin clearance, steady-state C-peptide/insulin molar ratio was lower in RD-fed and HF-fed *Cc1*$^{-/-}$ nulls, leading to chronic hyperinsulinemia (Table 1). This leads to insulin resistance [assessed by insulin intolerance (Fig. 1B) and fed hyperglycemia in RD-fed and HF-fed nulls relative to controls (Table 1)]. The mutation also caused glucose intolerance in response to both diets (Fig. 1B). In contrast to *Cc1*$^{+/+}$ and L-CC1 controls, HF caused fasting hyperglycemia in *Cc1*$^{-/-}$ nulls. Liver-specific redelivery of *Ceacam1* restored insulin clearance to reverse hyperinsulinemia and fed hyperglycemia (Table 1), and normalized insulin and glucose tolerance in RD-fed and HF-fed *Cc1*$^{-/-\text{xliver+}}$ mice (Fig. 1B). It also reversed diet-induced fasting hyperglycemia (Table 1) even after 5 months of HF intake (119±9 in *Cc1*$^{-/-\text{xliver+}}$ vs 154±7 in *Cc1*$^{-/-}$ mice).

3.2. Liver-specific reconstitution of CEACAM1 reversed diet-induced hepatic steatosis in null mice

Histological analysis of H&E-stained liver sections revealed diffuse microvesicular lipid droplets in the liver parenchyma of RD-fed *Cc1*$^{-/-}$ mice (Fig. 2A.iii) and a mixture of micro- and macrovesicular lipid deposits when fed HF (Fig. 2A.vii). This was supported by increased hepatic triglyceride without changes in total cholesterol levels (Table 1). Hepatic CEACAM1 restoration curbed lipid accumulation in RD- and HF-fed *Cc1*$^{-/-\text{xliver+}}$ mice (Fig. 2A.iv vs iii; viii vs vii), also evidenced by its ~1.5-to-2-fold lowering effect on total hepatic triglyceride levels (Table 1). Increased hepatic lipid accumulation in RD-fed and HF-fed *Cc1*$^{-/-}$ mice relative to *Cc1*$^{+/+}$ and L-CC1 controls stemmed from the combined effect of enhanced fatty acid transport (high Cd36 mRNA) in RD-fed (Table S3) and HF-fed null livers (Table S4); increased *de novo* lipogenesis [as demonstrated by higher fatty acid synthase (FASN) activity (Fig. 2B.i)] and reduced fatty acid β-oxidation (Fig. 2B.ii). Elevated FASN activity in *Cc1*$^{-/-}$ livers could stem from increased hyperinsulinemia-driven transcriptional upregulation by SREBP-1c (Table S3–S4). Reduced hepatic fatty acid β-

oxidation (Fig. 2B.ii) was consistent with the ~2-fold lower Fgf21 mRNA levels in RD-fed and HF-fed *Cc1*$^{-/-}$ mice relative to controls (Table S3–S4). Liver-specific CEACAM1 reconstitution attenuated lipogenesis as indicated by reversed Cd36 and Fasn mRNA levels (Table S3–S4) and normalized FASN activity (Fig. 2B.i) in response to both diets. It also induced hepatic fatty acid β-oxidation under both feeding conditions (Fig. 2B.ii), in part related to recovering Fgf21 expression levels (Table S3–S4, *Cc1*$^{-/-xliver+}$ vs *Cc1*$^{-/-}$). This demonstrated that reconstituting hepatic CEACAM1 blunted steatosis by reducing *de novo* lipogenesis and increasing fatty acid β-oxidation in *Cc1*$^{-/-xliver+}$ livers. Furthermore, it limited substrate redistribution to WAT and subsequently, visceral adiposity, lipolysis and NEFA transport to the liver.

3.3. Liver-specific rescuing of CEACAM1 reversed diet-induced hepatic inflammation in null mice

H&E staining revealed a few inflammatory infiltrates in RD-fed *Cc1*$^{-/-}$ livers with no significant change in hepatocellular architecture (Fig. 2A.iii). Consistent with lipotoxicity-driven inflammation, HF feeding increased perivascular and lobular inflammatory cell infiltrates in *Cc1*$^{-/-}$ livers by comparison to *Cc1*$^{+/+}$ and L-CC1 controls (Fig. 2A.vii). Liver-specific rescuing of CEACAM1 markedly curbed this inflammatory response to HF diet (Fig. 2A.viii vs vii, Table 3).

qRT-PCR analysis showed elevated total (F4/80) and activated (Cd68) macrophage pool, and neutrophil levels (Mpo, Elastase) in livers of null relative to controls fed RD or HF (Table S3–S4). Null livers also manifested higher mRNA of pro-inflammatory CD+4 and CD+8 T-lymphocytes with no increase in anti-inflammatory Treg pools (Foxp3; lL-10) (Table S3–S4). Higher hepatic Ifnγ, but not Il-4 and Il-13 mRNA levels in RD- and HF-fed null livers (Table S3–S4), indicated a $CD4^{+}$Th1 response. This pro-inflammatory state was marked by the activation of hepatic NF-κB in these mice (assessed by immunoblotting liver lysates with α-phosphoNF-κB normalized to loaded NF-κB, Fig. 2C). NF-κB induced the transcription of its targets, including pro-inflammatory cytokines such as Tnfα, Il-1β, and Il-6 (Table S3–S4), followed by their release, as manifested by elevated plasma TNFα and IL-6 levels (Table 2). IL-6 could, in turn, activate Stat3-mediated pro-inflammatory pathways (Fig. 2C) to synergize with TNFα activation of NF-κB to induce mRNA levels of Mcp-1/Ccl2 in monocytes/macrophages (Table S3–S4) and amplify their migration. Stat3 activation also represses interferon regulatory factor-8 (Irf-8) expression to upregulate the expression of Cd11b+ macrophages and granulocytes (Gr1 mRNA) (Table S3–S4) [28–30], thereby sustaining a pro-inflammatory state under both feeding conditions. Interestingly, liver-specific reconstitution of CEACAM1 reversed NF-κB and Stat3 activation (Fig. 2C), the rise in plasma TNFα and IL-6 (Table 2) and in the mRNA levels of pro-inflammatory cytokines and chemokines (Table S3–S4) under both feeding conditions. This lends further support to the critical role of hepatic CEACAM1 in regulating the inflammatory milieu of the liver [20].

In addition, HF amplified the activation of macrophages (F4/80, Cd68) and the production of pro-inflammatory cytokines (Tnfα, Il-1β; Il-6) in WAT of null mice (Table S5). This could promote a pro-inflammatory state (elevated plasma TNFα and IL-6) which synergized with

increased NEFA release to cause systemic insulin resistance in *Cc1*$^{-/-}$ mice compared to controls [31]. Liver-specific CEACAM1 reconstitution reversed this inflammatory response in WAT in mice fed either diet (Table S5, *Cc1*$^{-/-xliver+}$ vs *Cc1*$^{-/-}$).

3.4. Liver-specific redelivery of CEACAM1 in null mice reversed apoptosis, hepatic injury, and oxidative stress caused by high-fat diet

RD-fed and HF-fed *Cc1*$^{-/-}$ mice manifested liver dysfunction as assessed by their ~2-fold higher plasma alanine transaminase (ALT) and aspartate aminotransferase (AST) levels relative to controls (Table 2). Liver-specific CEACAM1 reconstitution normalized plasma ALT and AST levels and restored liver function (Table 2).

Apoptosis contributes to cell injury and liver dysfunction. Consistently, Tunel staining detected apoptotic cells in HF-fed null, but not control livers (Fig. 2D.vii). Moreover, mRNA level of *Chop*, an apoptosis marker, was induced by ~3-fold in HF-fed, but not in RD-fed *Cc1*$^{-/-}$ livers (Table S4–S3). This translated into higher hepatic CHOP protein content in HF-fed, but not RD-fed *Cc1*$^{-/-}$ mice (Fig. 2D). Together with the ~4-fold decrease in the expression of the anti-apoptosis Bcl2 gene in HF-fed nulls (Table S4), this pointed to the apoptosis-inducing effect of HF in null livers. qRT-PCR analysis revealed an ~2-to-3-fold increase in the expression of hepatic injury markers (Hgf, Nqo1, Nrf1) in RD-fed and HF-fed *Cc1*$^{-/-}$ livers (Table S3–S4).

Consistent with oxidative stress contributing to hepatocyte dysfunction [6], hepatic mRNA levels of NADPH oxidase (Nox1, Nox4) were elevated (Table S3–S4) and hepatic nitric oxide (NO) levels were lower in RD-fed and HF-fed nulls as compared to controls (Table 2), likely due to compromised activation of Akt/eNOS pathway in null livers [36] and as manifested by reduced basal eNOS phosphorylation (Fig. 2C). Additionally, RD-fed *Cc1*$^{-/-}$ livers manifested normal mRNA levels of Cyp2E1, a cytochrome p450 enzyme involved in the metabolism of long-chain fatty acids (lipooxygenation) and microsomal lipid ω-peroxidation (Table S3). HF induced Cyp2E1 mRNA by ~2-fold in *Cc1*$^{-/-}$, but not control livers (Table S4 vs S3), possibly by activating NF-κB pathways [32]. Moreover, HF lowered Npc1 mRNA in null livers by ~50%, contributing to reduced GSH levels (Table 2) and subsequently, increased response to the cytotoxic effect of elevated TNFα levels in null mice [33], which could in turn, activate IKK-β, a redox-sensitive kinase that upregulates NF-κB–dependent proinflammatory pathways [34]. In addition, HF, but not RD intake, induced PKCζ activation (phosphorylation) in null but not control mice (Fig. 2C). In light of PKCζ activation of NF-κB [35], its preferential phosphorylation in HF-fed nulls could contribute to diet-induced nitroso-redox imbalance and hepatocyte injury in null livers.

Liver-specific CEACAM1 reconstituted restored liver function even in response to HF (assessed by normalizing ALT and AST levels, Table 2). It reversed HF-induced apoptosis in *Cc1*$^{-/-xliver+}$ mice [reducing tunel stained cells, restoring Bcl2 and Chop expression (Table S3) and normalizing CHOP protein content (Fig. 2D)]. It also prevented oxidative stress and liver injury in RD-fed and HF-fed nulls (*Cc1*$^{-/-xliver+}$ vs *Cc1*$^{-/-}$ mice), as evidenced by normalized hepatic mRNA levels of Nox1 and Nox4 (Table S3–S4), and hepatic NO levels (Table 2); likely resulting from restored eNOS activation (phosphorylation) (Fig. 2C). This

assigns a major role for hepatic CEACAM1-dependent pathways in protecting against diet-induced hepatocyte injury and apoptosis.

3.5. Liver-specific reconstitution of CEACAM1 protected against fibrosis in null mice

As reported [22], Sirius red staining showed spontaneous and diet-amplified interstitial chicken-wire pattern of collagen deposition in *Cc1*$^{-/-}$ mice (Fig. 3A and accompanying table). These pathologies were reversed to control basal levels upon exclusive hepatic CEACAM1 rescuing (Fig. 3A.iv vs iii, viii vs vii-Table). Consistently, mRNA levels of pro-fibrogenic genes (Tgfβ, α-Sma, Ctgf) (Fig. 3B) and the protein content of α-SMA (Fig. 3C) were ≥2-fold higher in null livers relative to controls under both feeding conditions. This was mediated by TGFβ-Smad2/3 activation, as indicated by increased Smad2/3 phosphorylation (Fig. 3C) and by the ~3-to-4–fold decrease in the mRNA (Table S3–S4) and protein (Fig. 3C) levels of TGFβ-Smad2/3 inhibitor, Smad7, arising from elevated plasma and hepatic TNFα levels [36]. Liver-specific CEACAM1 rescuing reversed fibrosis caused by global *Ceacam1* null deletion even in HF-fed mice (Fig. 3A.iv and viii). This was mediated by inactivating TGFβ-Smad2/3 [blunted Smad2/3 phosphorylation (Fig. 3C) and restored hepatic Smad7 mRNA (Table S3–S4) and protein levels (Fig. 3C) in parallel to TNFα normalization].

As previously reported [37], *Cc1*$^{-/-}$ mice exhibited an increase in plasma endothelin-1 (Et-1) levels by 2-to-4–fold irrespective of the diet (Table 2), likely resulting from hyperinsulinemia [38], as evidenced by its reversal in *Cc1*$^{-/-xliver+}$ mice (Table 2). Hepatic mRNA levels of ET-1 and of its receptor A (*Etar*) that mediates its pro-fibrogenic activity (Fig. 3B) were elevated in *Cc1*$^{-/-}$ but not *Cc1*$^{-/-xliver+}$ mice. Mechanistically, this could be mediated by NF-κB activation, which in the presence of low NO levels and oxidative stress, could also induce the transcription of the pro-fibrogenic platelet-derived growth factor-B (PDGF-B) directly or indirectly by activating HIF-1α [39, 40], as manifested by their higher hepatic expression in null mice (Fig. 3B). Liver-specific rescuing of CEACAM1 normalized plasma (Table 2) and hepatic ET-1 and PDGF-B mRNA levels (Fig. 3B) via inactivating NF-κB and HIF-1α pathways in the normoinsulinemic (Fig. 2C–3C) and normoglycemic *Cc1*$^{-/-xliver+}$ mice.

HF feeding for 5 months caused similar molecular and histopathologic anomalies to 3 months of high-fat intake. Pertinent analyses are summarized through evaluating NAFLD activity score (NAS) per NIH guidelines (Table 3). As shown, RD-fed *Cc1*$^{-/-}$ mice did not exhibit the full spectrum of NASH even at 8 months of age (NAS<4). In contrast, HF feeding for 5 months caused a NAS score of >7 in nulls (Table 3). Liver-specific CEACAM1 rescuing restored NAS to <4 even after 5 months of HF and protected against NASH (Table 3).

3.7. Nicotinic acid treatment demonstrated a limited role for lipolysis in the pathogenesis of hepatic fibrosis in HF-fed Ceacam1 nulls

We next treated mice with nicotinic acid (NA) at the end of 5 months of HF feeding to reverse plasma NEFA (Fig. 4A) and adipokines (examplified by IL-6; Fig. 4B) in *Cc1*$^{-/-}$ by comparison to vehicle (Veh) treatment. Like in RD-fed *Cc1*$^{-/-}$ mice [25], NA did not reverse

hyperinsulinemia (Fig. 4C) or insulin resistance (Fig. 4D) in HF-fed *Cc1*$^{-/-}$ mice, as expected from the loss of hepatic Ceacam1 expression (Table S6). Accordingly, NA did not reverse diet-induced macrovesicular steatosis (Fig. 4E.iii) or mRNA levels of Srebp-1c in null livers (Fig. 4G). Consistent with lipolysis-derived NEFA driving fatty acid β-oxidation [41], NA normalized Cpt1 mRNA levels in null mice (Fig. 4G). Loss of macrosteatosis in HF-fed NA-treated *Cc1*$^{-/-\text{xliver}+}$ mice (Fig. 4G.iv vs iii) demonstrated that macrosteatosis in HF-fed *Cc1*$^{-/-}$ mice stemmed primarily from hepatic loss of CEACAM1.

Despite normalization of plasma cytokines by NA (Fig. 4B), mRNA levels of pro-inflammatory genes (Cd68, Tnfα, Il-1β, Il-6) remained elevated in NA-treated HF-fed null livers (Fig. 4G), resulting from NF-κB activation (Fig. 4H). Moreover, histopathological evaluation detected sustained robust lobular/portal inflammatory infiltration in HF-fed NA-treated null livers relative to other groups (Fig. 4E). Together with a steatosis score of 3, this maintained a NAS score of >7 in HF-fed NA-treated null mice (which was normalized to a NAS score of <4 in *Cc1*$^{-/-xliver}$ mice).

Sirius red staining showed persistent interstitial chicken-wire pattern of collagen deposition in HF-fed NA-treated *Cc1*$^{-/-}$ mice that was reversed by liver-specific CEACAM1 rescuing (Fig. 4F.iv vs iii, Brunt score of 1 vs 3). This was supported by sustained elevated expression of pro-fibrogenic genes (α-Sma, Et-1, Pdgf-B) (Fig. 4G) and the protein content of α-SMA (Fig.4H) in *Cc1*$^{-/-}$ versus *Cc1*$^{-/-xliver+}$ livers. Hepatic fibrosis in HF-fed NA-treated nulls was mediated by activation (phosphorylation) of TGFβ-Smad2/3 pathway, in turn upregulated by Smad7 loss (Fig. 4H). Reversal of NF-κB–driven hepatic pro-fibrogenic gene expression and TGFβ pathway activation by liver-specific CEACAM1 reconstitution supported the primary role of hepatic CEACAM1 in the pathogenesis of fibrosis in *Cc1*$^{-/-}$ mice.

4. Discussion

The metabolic and histopathological phenotypes of *Cc1*$^{-/-}$ [22] and L-SACC1 liver-specific inactive mice [42] provided an *in vivo* demonstration of the mechanistic underpinning of NASH. The causal role of impaired insulin clearance in insulin resistance and NAFLD was best manifested by the gradual progression of metabolic dysregulation in the liver-specific AlbCre+*Cc1*$^{fl/fl}$ null. This mouse developed impaired insulin clearance and chronic hyperinsulinemia at 2 months of age, followed by hepatic insulin resistance and steatosis. This increased substrate redistribution to WAT and subsequently, visceral obesity, lipolysis and systemic insulin resistance at 9 months of age [17]. Consistent with elevated pro-inflammatory response to steatosis, *Ceacam1* mutants developed spontaneous steatohepatitis [20, 23, 42]. In support of the well-documented role of inflammation in hepatocellular injury [43] and of the metabolic and immune regulation of liver function by CEACAM1 [24], they also developed oxidative stress and low-grade fibrosis that progressed into severe fibrosis when fed a HF diet [22, 42]. In contrast, the liver-specific gain-of-function model used in the current studies exhibited not only a reversal of the severe metabolic derangement amplified by prolonged HF intake in *Cc1*$^{-/-}$ mice, but also reversal of advanced hepatic fibrosis. Persistence of hepatic fibrosis in HF-diet nulls treated with nicotinic acid demonstrated that progressive fibrosis in *Cc1*$^{-/-}$ mice is primarily caused by the loss of hepatic CEACAM1

and that adipocytes-derived NEFA and adipokines did not contribute significantly to this phenotype. This provided an *in vivo* manifest of how the loss of hepatic CEACAM1 mediates, not only insulin resistance [25], and subsequently, steatosis-to-NAFLD switch, but also NASH escalation, including advanced fibrosis and apoptosis caused by HF intake.

As in L-SACC1 mutants [42], HF induced lipid peroxidation in *Cc1*$^{-/-}$ but not wild-type mice. This HF-induced nitroso-redox imbalance could initiate peroxidative events commonly associated with necrotic damage and apoptosis in null livers [1, 44]. This could be triggered in part by inducing hepatic TNFα [45] and amplifying its cytotoxic effect through the compromised GSH-based mitochondrial defense system associated with lower NPC1 and possible partitioning of free-cholesterol to mitochondria in *Cc1*$^{-/-}$ [44], as was shown for L-SACC1 mice [42]. Reversal of this phenotype by liver-specific reintroduction of CEACAM1 further underscored the role of CEACAM1 loss in the pathogenesis of oxidative stress and inflammation commonly implicated in NASH [3, 6, 28].

Fibrosis in *Cc1*$^{-/-}$ mice was mediated by activated TGFβ-Smad2/3 canonical pathways and driven by increased production of ET-1 and PDGF-B, two key pro-fibrogenic effectors. Increased levels of ET-1 could result from hyperinsulinemia [38], as supported by its normalization upon restoring normoinsulinemia and insulin sensitivity in *Cc1*$^{-/-\text{xliver}+}$ mice. As previously shown, Akt/eNOS-dependent NO synthesis was repressed in *Cc1*$^{-/-}$ vascular endothelium as a result of hyperinsulinemia-driven downregulation of insulin receptors [37]. The increase in ET-1 in the presence of low NO could result from NF-κB activation directly or indirectly via HIF-1α [39]. This could tip the vasomotor balance towards vasoconstriction, which could activate hepatic stellate cells to cause fibrosis [46].

Activated NF-κB (alone or jointly with HIF-1α) could induce PDGF-B transcription [39, 40]. Consistent with PKC inducing PDGF-B expression in fasting hyperglycemia [47], HF activated PKCζ in *Cc1*$^{-/-}$, but not control mice in parallel to increasing their lipid peroxidation. Elevated PDGF-B could synergize with ET-1 to induce collagen production by triggering proliferation of stellate cells [46]. Normalizing ET-1 and PDGF-B by curbing inflammation and oxidative stress in mice with liver-specific CEACAM1 redelivery prevented fibrosis. Reversal of NASH in *Cc1*$^{-/-}$ upon restoring their hepatic CEACAM1 expression emphasized the key role of hepatic CEACAM1 in maintaining normal liver architecture and function even under conditions of excess energy supply, and not just their insulin sensitivity.

5. Strengths and weaknesses

Contrary to recent reports showing a critical role for adipocytes-derived effectors in hepatic fibrosis in humans [48], the current studies showed that blocking lipolysis and adipokines release from adipose tissue did not limit hepatic fibrosis in *Cc1*$^{-/-}$ mice. Nevertheless, the current studies identified hepatic CEACAM1 as a defense system against diet-induced liver fibrosis, as previously shown for WAT fibrosis [49]. In support of these findings, liver grafts with low CEACAM1 manifested an increase in ischemia-reperfusion injury inflammation and decreased function in wild-type recipient mice and caused post-reperfusion damage in liver transplant human recipients [50]. Interestingly, PPARγ and GLP-1 receptor agonists

that are used to treat insulin-resistant NAFLD patients [9, 10] with advanced fibrosis [51] induce Ceacam1 transcription [52]. Thus, it is likely that the effectiveness of these drugs is mediated partly by their positive effect on CEACAM1 expression. Thus, inducing hepatic CEACAM1 expression could constitute an efficacious targeted therapeutical approach not only to curb insulin resistance and NAFLD, but also to prevent or reverse fibrosis without causing the body weight gain often observed in patients treated with PPARγ agonists. Drug development followed by clinical studies are needed to test this postulation.

6. Conclusions

The current studies demonstrated that liver-specific reconstitution of CEACAM1 in *Cc1*$^{-/-}$ nulls reversed hyperinsulinemia-driven histopathological features of NASH and prevented hepatic fibrosis and dysfunction. This proposes that targeting CEACAM1 could constitute a novel therapeutic approach against NASH and its esacalation to end-stage liver disease.

Supplementary Material

Refer to Web version on PubMed Central for supplementary material.

Acknowledgments

The authors thank Ms Julie Buckley at the Ohio University Histopathology Facility for her technical assistance in histological analysis and staining. They also thank Dr. Amal K. Najjar, visiting Fulbright Scholar, for critical reading of the manuscript.

Financial support:

This work was supported by the National Institutes of Health [grants: R01-HL112248, R01-DK054254, R01-DK083850 and R01DK124126 to S.M.N]. The work was also partly supported by the Middle East Diabetes Research Center to H.E.G.

NON-STANDARD ABBREVIATIONS

ALT	Alanine aminotransferase
AST	Aspartate aminotransferase
CEACAM1	Carcinoembryonic Antigen-related Cell Adhesion Molecule 1
Ceacam1 (Cc1)	Gene encoding CEACAM1 protein
Cc1	*Ceacam1* gene
Cc1$^{-/-}$	Global *Ceacam1* homozygous null mutant mice
L-CC1	Wild-type mice with forced liver-specific overexpression of rat *Ceacam1* transgene driven by Apolipoprotein A1 promoter
Cc1$^{-/-\text{xliver}+}$	Cc1$^{-/-}$ mice with transgenic liver-specific reconstitution of rat *Ceacam1* transgene

ET-1	Endothelin-1
ETAR/ETBR	Endothelin-1 Receptor-A/B isoforms
GSH	Reduced glutathione
HF	High-fat diet
HIF-1α	Hypoxia-inducible factor-1alpha
IL-6	Interleukin-6
NEFA	Non-esterified fatty acids
NA	Nicotinic acid
NO	Nitric oxide
NPC1	Niemann Pick type C1
PDGF-B	Platelet-derived growth factor-B
RD	Regular chow diet
TGFβ	Transforming growth factor beta
TNFα	Tumor necrosis factor alpha
WAT	White adipose tissue

References

[1]. Buzzetti E, Pinzani M, Tsochatzis EA. The multiple-hit pathogenesis of non-alcoholic fatty liver disease (NAFLD). Metabolism. 2016;65:1038–48. [PubMed: 26823198]

[2]. Younossi ZM. Non-alcoholic fatty liver disease - A global public health perspective. J Hepatol. 2019;70:531–44. [PubMed: 30414863]

[3]. Tilg H, Moschen AR. Evolution of inflammation in nonalcoholic fatty liver disease: the multiple parallel hits hypothesis. Hepatology. 2010;52:1836–46. [PubMed: 21038418]

[4]. Gan LT, Van Rooyen DM, Koina ME, McCuskey RS, Teoh NC, Farrell GC. Hepatocyte free cholesterol lipotoxicity results from JNK1-mediated mitochondrial injury and is HMGB1 and TLR4-dependent. J Hepatol. 2014;61:1376–84. [PubMed: 25064435]

[5]. Fuchs M, Sanyal AJ. Lipotoxicity in NASH. J Hepatol. 2012;56:291–3. [PubMed: 21741924]

[6]. Dallio M, Sangineto M, Romeo M, Villani R, Romano AD, Loguercio C, et al. Immunity as Cornerstone of Non-Alcoholic Fatty Liver Disease: The Contribution of Oxidative Stress in the Disease Progression. Int J Mol Sci. 2021;22.

[7]. Masarone M, Rosato V, Dallio M, Gravina AG, Aglitti A, Loguercio C, et al. Role of Oxidative Stress in Pathophysiology of Nonalcoholic Fatty Liver Disease. Oxid Med Cell Longev. 2018;2018:9547613. [PubMed: 29991976]

[8]. Thomas DD, Corkey BE, Istfan NW, Apovian CM. Hyperinsulinemia: An Early Indicator of Metabolic Dysfunction. J Endocr Soc. 2019;3:1727–47. [PubMed: 31528832]

[9]. Gastaldelli A, Cusi K. From NASH to diabetes and from diabetes to NASH: Mechanisms and treatment options. JHEP Rep. 2019;1:312–28. [PubMed: 32039382]

[10]. Stefan N, Haring HU, Cusi K. Non-alcoholic fatty liver disease: causes, diagnosis, cardiometabolic consequences, and treatment strategies. Lancet Diabetes Endocrinol. 2019;7:313–24. [PubMed: 30174213]

[11]. Bril F, Lomonaco R, Orsak B, Ortiz-Lopez C, Webb A, Tio F, et al. Relationship between disease severity, hyperinsulinemia, and impaired insulin clearance in patients with nonalcoholic steatohepatitis. Hepatology. 2014;59:2178–87. [PubMed: 24777953]

[12]. Heinrich G, Muturi HT, Rezaei K, Al-Share QY, DeAngelis AM, Bowman TA, et al. Reduced hepatic carcinoembryonic antigen-related cell adhesion molecule 1 level in obesity. Front Endocrinol (Lausanne). 2017;8:54. [PubMed: 28396653]

[13]. Lee W The CEACAM1 expression is decreased in the liver of severely obese patients with or without diabetes. Diagn Pathol. 2011;6:40. [PubMed: 21569294]

[14]. Najjar SM, Perdomo G. Hepatic Insulin Clearance: Mechanism and Physiology. Physiology (Bethesda). 2019;34:198–215. [PubMed: 30968756]

[15]. Xu E, Dubois MJ, Leung N, Charbonneau A, Turbide C, Avramoglu RK, et al. Targeted disruption of carcinoembryonic antigen-related cell adhesion molecule 1 promotes diet-induced hepatic steatosis and insulin resistance. Endocrinology. 2009;150:3503–12. [PubMed: 19406938]

[16]. DeAngelis AM, Heinrich G, Dai T, Bowman TA, Patel PR, Lee SJ, et al. Carcinoembryonic antigen-related cell adhesion molecule 1: a link between insulin and lipid metabolism. Diabetes. 2008;57:2296–303. [PubMed: 18544705]

[17]. Ghadieh HE, Russo L, Muturi HT, Ghanem SS, Manaserh IH, Noh HL, et al. Hyperinsulinemia drives hepatic insulin resistance in male mice with liver-specific Ceacam1 deletion independently of lipolysis. Metabolism. 2019;93:33–43. [PubMed: 30664851]

[18]. Poy MN, Yang Y, Rezaei K, Fernstrom MA, Lee AD, Kido Y, et al. CEACAM1 regulates insulin clearance in liver. Nat Genet. 2002;30:270–6. [PubMed: 11850617]

[19]. Najjar SM, Yang Y, Fernstrom MA, Lee SJ, Deangelis AM, Rjaily GA, et al. Insulin acutely decreases hepatic fatty acid synthase activity. Cell Metab. 2005;2:43–53. [PubMed: 16054098]

[20]. Najjar SM, Russo L. CEACAM1 loss links inflammation to insulin resistance in obesity and non-alcoholic steatohepatitis (NASH). Semin Immunopathol. 2014;36:55–71. [PubMed: 24258517]

[21]. Najjar SM, Ledford KJ, Abdallah SL, Paus A, Russo L, Kaw MK, et al. Ceacam1 deletion causes vascular alterations in large vessels. Am J Physiol Endocrinol Metab. 2013;305:E519–29. [PubMed: 23800882]

[22]. Ghosh S, Kaw M, Patel PR, Ledford KJ, Bowman TA, McLnerney MF, et al. Mice with null mutation of Ceacam I develop nonalcoholic steatohepatitis. Hepat Med: Res Evidence. 2010;2010:69–78.

[23]. Ghadieh HE, Abu Helal R, Muturi HT, Issa DD, Russo L, Abdallah SL, et al. Loss of Hepatic Carcinoembryonic Antigen-Related Cell Adhesion Molecule 1 Links Nonalcoholic Steatohepatitis to Atherosclerosis. Hepatol Commun. 2020;4:1591–609. [PubMed: 33163831]

[24]. Horst AK, Najjar SM, Wagener C, Tiegs G. CEACAM1 in Liver Injury, Metabolic and Immune Regulation. Int J Mol Sci. 2018;19.

[25]. Russo L, Muturi HT, Ghadieh HE, Ghanem SS, Bowman TA, Noh HL, et al. Liver-specific reconstitution of CEACAM1 reverses the metabolic abnormalities caused by its global deletion in male mice. Diabetologia. 2017;60:2463–74. [PubMed: 28913658]

[26]. Al-Share QY, DeAngelis AM, Lester SG, Bowman TA, Ramakrishnan SK, Abdallah SL, et al. Forced Hepatic Overexpression of CEACAM1 Curtails Diet-Induced Insulin Resistance. Diabetes. 2015;64:2780–90. [PubMed: 25972571]

[27]. Santiago-Rolon A, Purcell D, Rosado K, Toro DH. A Comparison of Brunt's Criteria, the Non-Alcoholic Fatty Liver Disease Activity Score (NAS), and a Proposed NAS Scoring that Includes Fibrosis in Non-Alcoholic Fatty Liver Disease Staging. Puerto Rico Health Sci J. 2015;34:189–94.

[28]. Tacke F, Zimmermann HW. Macrophage heterogeneity in liver injury and fibrosis. J Hepatol. 2014;60:1090–6. [PubMed: 24412603]

[29]. Adelaja A, Hoffmann A. Signaling Crosstalk Mechanisms That May Fine-Tune Pathogen-Responsive NFkappaB. Front Immunol. 2019;10:433. [PubMed: 31312197]

[30]. Suryavanshi SV, Kulkarni YA. NF-kappabeta: A Potential Target in the Management of Vascular Complications of Diabetes. Front Pharmacol. 2017;8:798. [PubMed: 29163178]

[31]. Gregor MF, Hotamisligil GS. Inflammatory mechanisms in obesity. Ann Rev Immunol. 2011;29:415–45. [PubMed: 21219177]

[32]. Abdel-Razzak Z, Garlatti M, Aggerbeck M, Barouki R. Determination of interleukin-4-responsive region in the human cytochrome P450 2E1 gene promoter. Biochem Pharmacol. 2004;68:1371–81. [PubMed: 15345327]

[33]. Mari M, Caballero F, Colell A, Morales A, Caballeria J, Fernandez A, et al. Mitochondrial free cholesterol loading sensitizes to TNF- and Fas-mediated steatohepatitis. Cell Metab. 2006;4:185–98. [PubMed: 16950136]

[34]. Cai D, Yuan M, Frantz DF, Melendez PA, Hansen L, Lee J, et al. Local and systemic insulin resistance resulting from hepatic activation of IKK-beta and NF-kappaB. Nat Med. 2005;11:183–90. [PubMed: 15685173]

[35]. Manicassamy S, Gupta S, Huang Z, Sun Z. Protein kinase C-theta-mediated signals enhance CD4+ T cell survival by up-regulating Bcl-xL. J Immunol. 2006;176:6709–16. [PubMed: 16709830]

[36]. Nagarajan RP, Chen F, Li W, Vig E, Harrington MA, Nakshatri H, et al. Repression of transforming-growth-factor-beta-mediated transcription by nuclear factor kappaB. Biochem J. 2000;348 Pt 3:591–6. [PubMed: 10839991]

[37]. Russo L, Muturi HT, Ghadieh HE, Wisniewski AM, Morgan EE, Quadri SS, et al. Liver-specific rescuing of CEACAM1 reverses endothelial and cardiovascular abnormalities in male mice with null deletion of Ceacam1 gene. Mol Metab. 2018;9:98–113. [PubMed: 29396368]

[38]. Mahmoud AM, Szczurek MR, Blackburn BK, Mey JT, Chen Z, Robinson AT, et al. Hyperinsulinemia augments endothelin-1 protein expression and impairs vasodilation of human skeletal muscle arterioles. Physiol Rep. 2016;4.

[39]. van Uden P, Kenneth NS, Rocha S. Regulation of hypoxia-inducible factor-1alpha by NF-kappaB. Biochem J. 2008;412:477–84. [PubMed: 18393939]

[40]. Au PY, Martin N, Chau H, Moemeni B, Chia M, Liu FF, et al. The oncogene PDGF-B provides a key switch from cell death to survival induced by TNF. Oncogene. 2005;24:3196–205. [PubMed: 15735680]

[41]. Titchenell PM, Quinn WJ, Lu M, Chu Q, Lu W, Li C, et al. Direct hepatocyte insulin signaling is required for lipogenesis but is dispensable for the suppression of glucose production. Cell Metab. 2016;23:1154–66. [PubMed: 27238637]

[42]. Lee SJ, Heinrich G, Fedorova L, Al-Share QY, Ledford KJ, Fernstrom MA, et al. Development of nonalcoholic steatohepatitis in insulin-resistant liver-specific S503A carcinoembryonic antigen-related cell adhesion molecule 1 mutant mice. Gastroenterology. 2008;135:2084–95. [PubMed: 18848945]

[43]. Wan J, Weiss E, Ben Mkaddem S, Mabire M, Choinier PM, Thibault-Sogorb T, et al. LC3-associated phagocytosis in myeloid cells, a fireman that restrains inflammation and liver fibrosis, via immunoreceptor inhibitory signaling. Autophagy. 2020;16:1526–8. [PubMed: 32434445]

[44]. Musso G, Gambino R, Cassader M. Cholesterol metabolism and the pathogenesis of non-alcoholic steatohepatitis. Prog Lipid Res. 2013;52:175–91. [PubMed: 23206728]

[45]. Carter-Kent C, Zein NN, Feldstein AE. Cytokines in the pathogenesis of fatty liver and disease progression to steatohepatitis: implications for treatment. Am J Gastroenterol. 2008;103:1036–42. [PubMed: 18177455]

[46]. Friedman SL. Mechanisms of hepatic fibrogenesis. Gastroenterology. 2008;134:1655–69. [PubMed: 18471545]

[47]. Yokota T, Ma RC, Park JY, Isshiki K, Sotiropoulos KB, Rauniyar RK, et al. Role of protein kinase C on the expression of platelet-derived growth factor and endothelin-1 in the retina of diabetic rats and cultured retinal capillary pericytes. Diabetes. 2003;52:838–45. [PubMed: 12606528]

[48]. Rosso C, Kazankov K, Younes R, Esmaili S, Marietti M, Sacco M, et al. Crosstalk between adipose tissue insulin resistance and liver macrophages in non-alcoholic fatty liver disease. J Hepatol. 2019;71:1012–21. [PubMed: 31301321]

[49]. Lester SG, Russo L, Ghanem SS, Khuder SS, DeAngelis AM, Esakov EL, et al. Hepatic CEACAM1 over-expression protects against diet-induced fibrosis and inflammation in white adipose tissue. Front Endocrinol (Lausanne). 2015;6:116–22. [PubMed: 26284027]

[50]. Nakamura K, Kageyama S, Kaldas FM, Hirao H, Ito T, Kadono K, et al. Hepatic CEACAM1 expression indicates donor liver quality and prevents early transplantation injury. J Clin Invest. 2020;130:2689–704. [PubMed: 32027621]

[51]. Musso G, Cassader M, Paschetta E, Gambino R. Pioglitazone for advanced fibrosis in nonalcoholic steatohepatitis: New evidence, new challenges. Hepatology. 2017;65:1058–61. [PubMed: 27880988]

[52]. Ghadieh HE, Muturi HT, Russo L, Marino CC, Ghanem SS, Khuder SS, et al. Exenatide induces carcinoembryonic antigen-related cell adhesion molecule 1 expression to prevent hepatic steatosis. Hepatol Commun. 2018;2:35–47. [PubMed: 29404511]

HIGHLIGHTS

- Hepatic fibrosis in *Cc1*$^{-/-}$ mice is primarily caused by loss of hepatic CEACAM1
- Fibrosis is mediated by activated NF-kB–triggered fibrogenic gene transcription
- Liver-specific reconstitution of CEACAM1 reverses NAFLD/NASH in HF-fed *Cc1*$^{-/-}$ mice
- Liver-specific reconstitution of CEACAM1 reverses fibrosis in HF-fed *Cc1*$^{-/-}$ mice
- Liver-specific reconstitution of CEACAM1 restores liver function in HF-fed *Cc1*$^{-/-}$ mice

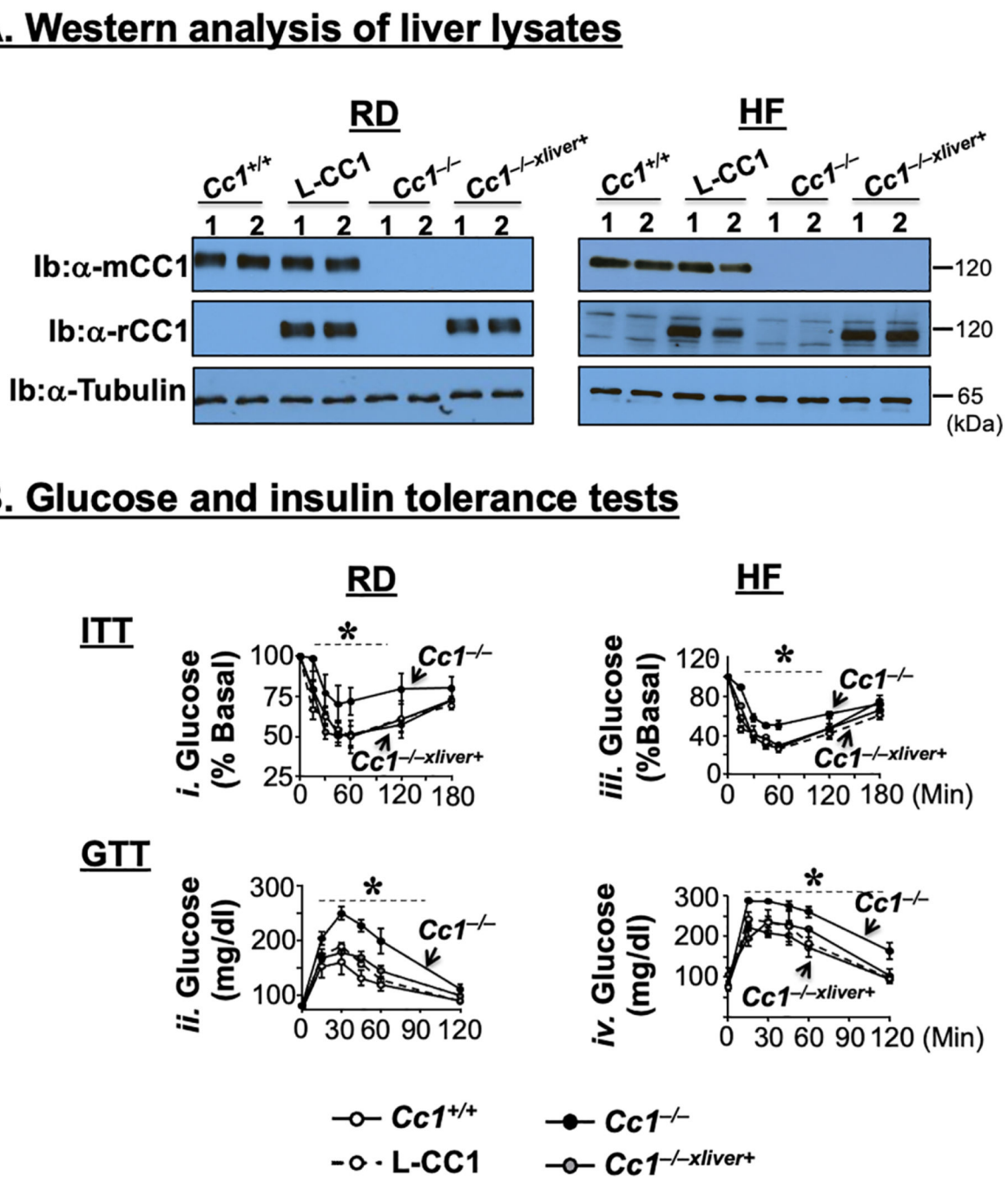

Fig. 1.

Expression and metabolic analysis. 3-month-old male mice were fed RD or HF diet for 3 months (n>5 per genotype/feeding group). (A) CEACAM1 protein level was analysed by immunoblotting (Ib) liver lysates with polyclonal antibodies against mouse (α-mCC1) or rat (α-rCC1) CEACAM1. To normalize against protein loading, the lower half of the membrane was immunoblotted with α-Tubulin. Numbers to the right of the gels indicate apparent molecular mass (kDa). Gels represent 2 experiments performed on 2 different mice/genotype. (B) mice were subjected to an intraperitoneal injection of insulin (0.75 U/kg BW)

(panels *i, iii*), and glucose (1.5 g/kg BW) (panels *ii* and *iv*) to evaluate blood glucose levels at 0–180 or 0–120 min post-injection, respectively.

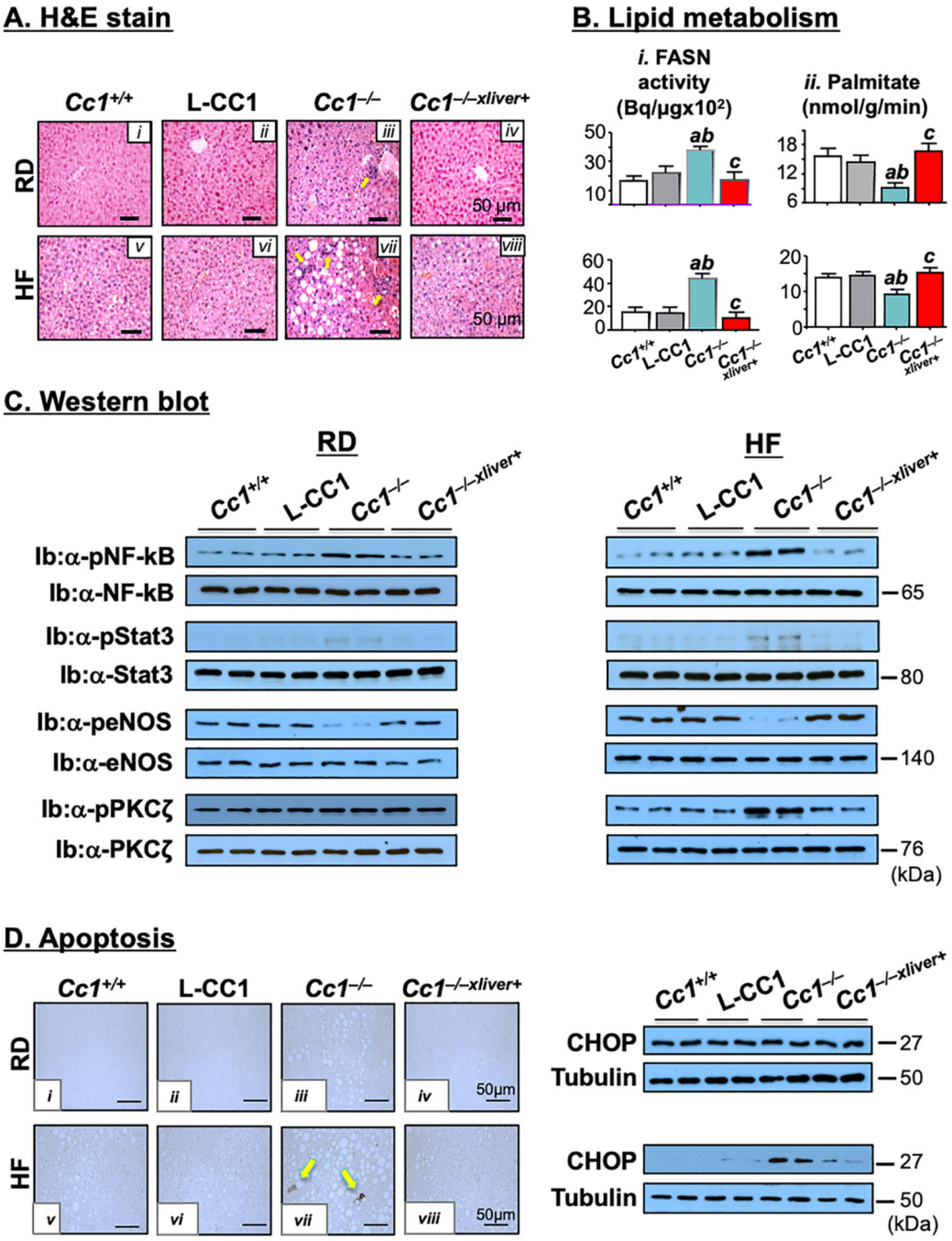

Fig. 2.

Histological and biochemical analysis. Livers of 6-month-old mice (n≥5/genotype) were extracted and sectioned for (A) H&E staining to detect inflammatory foci (yellow arrows) and microvesicular lipid droplets. Representative images are shown. (B) Hepatic fatty acid synthase (FASN) activity (panel *i*) and hepatic palmitate oxidation (panel *ii*) were assayed in overnight fasted RD-fed (upper graphs) and HF-fed mice (lower graphs). Assays were performed in triplicate. Values are expressed as means ± SEM. [a]$P<0.05$ vs $Cc1^{+/+}$; [b]$P<0.05$ vs L-CC1; and [c]$P<0.05$ vs $Cc1^{-/-}$. (C) Western blot analysis was performed on liver lysates

by immunoblotting (Ib) with antibodies against phosphorylated signaling proteins (α-pNF-κB, α-pStat3, α-peNOS, α-pPKCζ) normalized against their non-phosphorylated counterparts immunodetected on parallel gels. Numbers to the right of the gels indicate apparent molecular mass (kDa). Gels represent 2 experiments performed on 2 different mice/genotype. (D) Tunnel staining on liver sections to detect apoptotic bodies(yellow arrows) in RD-fed and HF-fed mice. Representative images are shown. CHOP protein was detected by immunoblotting with α-CHOP antibody normalized against total protein (α-Tubulin) loaded on parallel gel. Numbers to the right of the gels indicate apparent molecular mass (kDa). Gels represent 2 experiments performed on different mice/genotype.

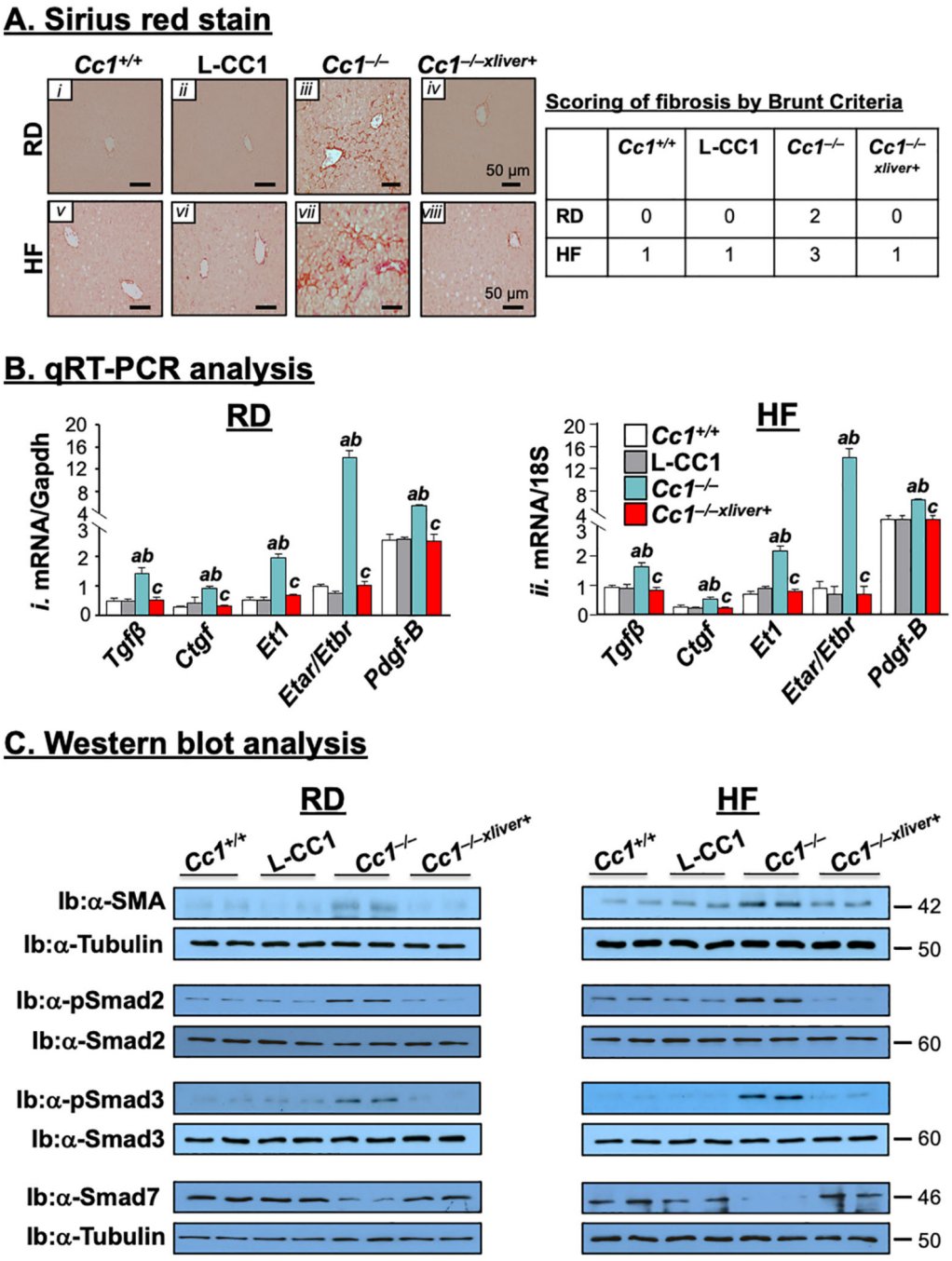

	Cc1+/+	L-CC1	Cc1−/−	Cc1−/− xliver+
RD	0	0	2	0
HF	1	1	3	1

Fig. 3.

Analysis of of hepatic fibrosis. Mice were fed RD or HF for 3 months (n≥5/genotype/feeding group). (A) Sirius red staining on liver sections was performed to detect interstitial collagen deposition in the parenchyma of *Cc1*$^{-/-}$ mice. Representative images are shown. Fibrosis scoring was evaluated by Brunt criteria in the accompanying table. (B) mRNA analysis of fibrotic markers in liver tissues from of RD or HF-fed mice normalized to Gapdh (RD) or 18S (HF). Values are expressed as means ± SEM. [a]*P*<0.05 vs *Cc1*$^{+/+}$; [b]*P*<0.05 vs L-CC1; and [c]*P*<0.05 vs *Cc1*$^{-/-}$. (C) Western blot analysis was performed on liver lysates by

immunoblotting (Ib) with antibodies against phosphorylated signaling proteins (α-pSmad2, α-pSmad3) normalized against their non-phosphorylated counterparts immunodetected on parallel gels. Smad7 and SMA proteins were detected by immunoblotting with α-Smad7 or α-SMA antibodies normalized against Tubulin on parallel gels. Gels represent more than 2 experiments performed on different mice/genotype.

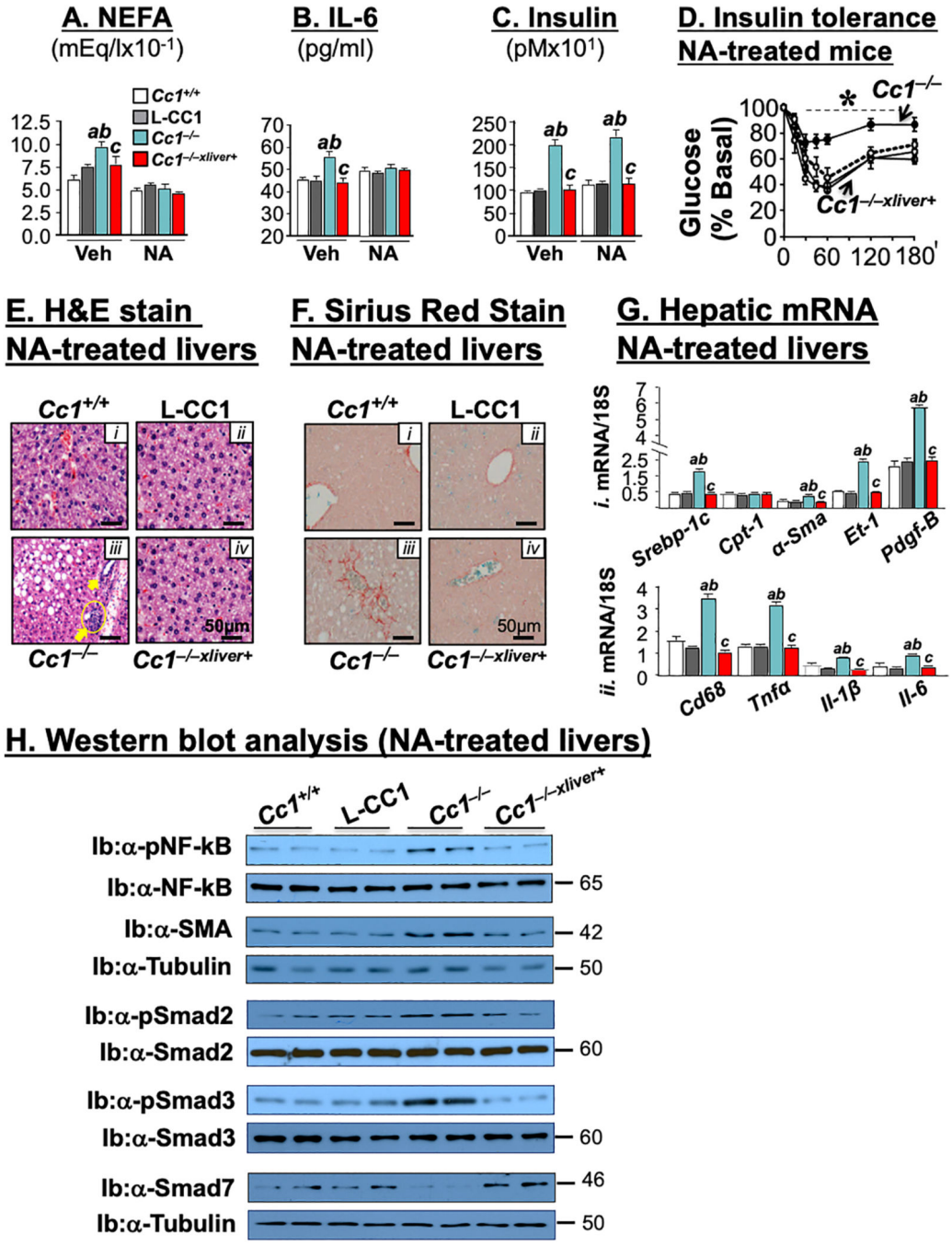

Fig. 4.

The effect of nicotinic acid on hepatic fibrosis. 3-month-old male mice were fed a HF diet for 5 months. (A) HF-fed mice were treated with vehicle (Veh) or once daily injection of nicotinic acid (NA) for 2 days before mice were sacrificed and blood and tissues were collected (n≥4 mice/genotype/treatment). Plasma (A) NEFA, (B) IL-6 and (C) insulin were measured in duplicate. Values are expressed as means ± SEM. [a]P<0.05 vs $Cc1^{+/+}$; [b]P<0.05 vs L-CC1; and [c]P<0.05 vs $Cc1^{-/-}$. (D) intraperitoneal Insulin tolerance test was used to assess insulin response, as in the legend to Fig. 1. *P<0.05 vs $Cc1^{-/-}$. (E) Livers of HF-fed

NA-treated mice were sectioned for H&E staining to detect macrovesicular steatosis and inflammation (yellow arrows). Representative images are shown. (F) Sirius red staining of liver sections was used to detect collagen deposition in the parenchyma of mice. Representative images are shown. (G) mRNA analysis of representative genes involved in lipid metabolism, fibrosis, and inflammation in HF-fed NA-treated livers normalized to 18S. Values are expressed as means ± SEM. [a]$P<0.05$ vs $Cc1^{+/+}$; [b]$P<0.05$ vs L-CC1; and [c]$P<0.05$ vs $Cc1^{-/-}$. (H) Western blot analysis was performed on liver lysates as in the legend to Fig. 3.

Table 1

Plasma and tissue metabolic parameters

	Cc1$^{+/+}$	L-CC1	*Cc1*$^{-/-}$	*Cc1*$^{-/-xliver+}$
a) RD				
% Fat mass	12.6 ± 0.6	11.3 ± 0.4	17.2 ± 0.6 *ab*	13.1 ± 0.1 *c*
% Lean mass	72.5 ± 1.0	77.0 ± 2.1	63.7 ± 1.0 *ab*	73.1 ± 1.3 *c*
Plasma NEFA (mEq/l)	0.5 ± 0.0	0.5 ± 0.1	1.0 ± 0.1 *ab*	0.4 ± 0.2 *c*
Plasma Insulin (pM)	76.6 ± 1.2	74.4 ± 1.0	140.6 ± 5.1 *ab*	74.1 ± 0.8 *c*
Plasma C-peptide (pM)	433.7 ± 1.9	415.8 ± 11.6	583.7 ± 3.1 *ab*	431.6 ± 0.4 *c*
C-peptide/Insulin	5.7 ± 0.1	5.6 ± 0.2	4.0 ± 0.1 *ab*	5.8 ± 0.1 *c*
Fasting blood glucose (mg/dl)	95 ± 8	75 ± 7	89 ± 2	73 ± 8
Fed blood glucose (mg/dl)	104 ± 9	93 ± 5	152 ± 7 *ab*	85 ± 5 *c*
Hepatic triglycerides (μg/mg)	59.1 ± 4.3	57.8 ± 1.1	84.1 ± 7.1 *ab*	57.9 ± 6.1 *c*
Plasma triglycerides (mg/dl)	51.4 ± 0.7	50.7 ± 2.1	51.9 ± 0.8	49.9 ± 1.1
Hepatic total cholesterol (mg/dl)	71 ± 6.1	75.7 ± 3.9	75.3 ± 3.4	75.3 ± 3.4
b) HF				
% Fat mass	25.4 ± 0.6	26.9 ± 0.4	30.6 ± 0.5 *ab*	24.5 ± 1.1 *c*
% Lean mass	59.5 ± 0.7	59.5 ± 1.0	54.1 ± 0.6 *ab*	62. ± 1.0 *c*
Plasma NEFA (mEq/l)	0.6 ± 0.2	0.6 ± 0.1	1.3 ± 0.1 *ab*	0.5 ± 0.2 *c*
Plasma Insulin (pM)	107.3 ± 5.9	104.4 ± 10.6	210.4 ± 3.8 *ab*	94.7 ± 2.2 *c*
Plasma C-peptide (pM)	696.7 ± 20.0	701.8 ± 11.4	1065 ± 32.1 *ab*	690.3 ± 1.7 *c*
C-peptide/Insulin	6.9 ± 0.6	7.4 ± 0.3	4.9 ± 0.2 *ab*	7.3 ± 0.2 *c*
Fasting blood glucose (mg/dl)	116 ± 6	120 ± 9	157 ± 7 *ab*	120 ± 5 *c*
Fed blood glucose (mg/dl)	116 ± 1	122 ± 8	171 ± 5 *ab*	114 ± 1 *c*
Hepatic triglycerides (μg/mg)	95.5 ± 3.6	76.0 ± 5.5	169.6 ± 30.5 *ab*	82.3 ± 3.5 *c*
Plasma triglycerides (mg/dl)	52.2 ± 0.9	47.7 ± 1.2	45.7 ± 0.9	43.7 ± 2.7
Hepatic total cholesterol (mg/dl)	81.2 ± 4.0	82.4 ± 2.5	84 ± 2.8	79.2 ± 4.4

Male mice were fed a HF or kept on RD diet for 3 months starting at 3 months of age (n≥5–8 mice/genotype/feeding group). Retro-orbital blood and tissues were collected at 11:00 a.m. following an overnight fast. Steady-state-C-peptide/insulin was calculated as a measure of insulin clearance. Values are expressed as mean±SEM.

a P<0.05 vs Cc1$^{+/+}$

b *P<0.05 vs* L-CC1

c P<0.05 vs Cc1$^{-/-}$.

Table 2

Plasma and tissue biochemistry

	Cc1$^{+/+}$	L-CC1	*Cc1*$^{-/-}$	*Cc1*$^{-/-xliver+}$
a) RD				
Plasma TNFα (pg/ml)	4.6 ± 0.2	4.7 ± 0.2	9.0 ± 0.1 *ab*	4.5 ± 0.3 *c*
Plasma IL-6 (pg/ml)	34.6 ± 1.4	34.0 ± 0.7	57.1 ± 2.1 *ab*	33.8 ± 1.0 *c*
Plasma AST (mU/ml)	44.7 ± 5.2	36.7 ± 6.4	87.7 ± 5.0 *ab*	48.9 ± 7.5 *c*
Plasma ALT (mU/ml)	7.7 ± 1.2	8.2 ± 1.0	14.8 ± 0.5 *ab*	9.3 ± 1.5 *c*
Hepatic NO (uM/ugx 10^{-1})	4.0 ± 0.0	4.0 ± 0.0	2.0 ± 0.0 *ab*	3.0 ± 0.0 *c*
Hepatic GSH (umol/g wt)	1.8 ± 0.1	1.8 ± 0.0	1.8 ± 0.0	1.7 ± 0.0
Plasma ET-1 (pg/ml)	4.2 ± 0.4	3.6 ± 0.8	11.7 ± 0.4 *ab*	4.6 ± 0.5 *c*
b) HF				
Plasma TNFα (pg/ml)	5.0 ± 0.2	5.5 ± 0.4	9.7 ± 0.3 *ab*	4.9 ± 0.2 *c*
Plasma IL-6 (pg/ml)	40.3 ± 1.3	39.8 ± 3.2	63.7 ± 1.7 *ab*	36.0 ± 2.5 *c*
Plasma AST (mU/ml)	77.6 ± 8.2	70.2 ± 9.6	135.7 ± 17.0 *ab*	58.9 ± 10.1 *c*
Plasma ALT (mU/ml)	16.8 ± 2.4	15.1 ± 1.6	27.0 ± 2.5 *ab*	13.4 ± 2.5 *c*
Hepatic NO (uM/ugx10^{-1})	5.0 ± 0.0	4.0 ± 0.0	2.0 ± 0.0 *ab*	5.0 ± 0.0 *c*
Hepatic GSH (umol/g wt)	4.3 ± 0.2	4.3 ± 0.2	1.6 ± 0.0 *ab*	4.3 ± 0.2 *c*
Plasma ET-1 (pg/ml)	15.6 ± 2.1	15.2 ± 2.4	33.7 ± 3.4 *ab*	13.6 ± 3.6 *c*

Male mice were fed a HF or kept on RD diet for 3 months starting at 3 months of age (n≥5–8 mice/genotype/feeding group). Retro-orbital blood and tissues were collected at 11:00 a.m. following an overnight fast. Values are expressed as mean±SEM.

a P<0.05 vs Cc1$^{+/+}$

b *P<0.05 vs* L-CC1

c P<0.05 vs Cc1$^{-/-}$.

Table 3

NAFLD activity score (NAS)

Group	Diet	Mice/number	Steatosis	Inflammation		Ballooning	Total NAS	NASH
			Micro/ macro (0–3)	Lobular (0–3)	Portal (0–3)	Hepatocyte (0–2)	Score (0–8)	
Cc1$^{+/+}$	RD	>3	0	≤ 1	0	0	≤ 1	No
Cc1$^{+/+}$	HF	>3	2	≤ 2	0	0	≤ 4	No
L-CC1	RD	>4	0	≤ 1	0	0	≤ 1	No
L-CC1	HF	>3	2	≤ 2	0	0	≤ 4	No
Cc1$^{-/-}$	RD	>3	≤ 2	1	≤ 1	0	≤ 4	No
Cc1$^{-/-}$	HF	>3	3	2	≤ 2	0	≤ 7	YES
Cc1$^{-/-xliver+}$	RD	>3	0	≤ 1	0	0	≤ 1	No
Cc1$^{-/-xliver+}$	HF	>3	2	≤ 2	0	0	≤ 4	No

Male mice were fed a HF or kept on RD diet for 5 months starting at 3 months of age (n≥3–6 mice/genotype/feeding group). NAS score was evaluated based on NIH guidelines. Score did not significantly change after nicotinic acid treatment.